

---

---

# Measuring fine molecular structures with luminescence signal from an alternating current scanning tunneling microscope

Fei Wen<sup>1</sup>, Guohui Dong<sup>2†</sup> and Hui Dong<sup>1†</sup>

<sup>1</sup> Graduate School of China Academy of Engineering Physics, Beijing 100084, China

<sup>2</sup> School of Physics and Electronic Engineering, Sichuan Normal University, Chengdu 610068, China

(Received XXXX; revised manuscript received XXXX)

In scanning tunneling microscopy induced luminescence (STML), the photon counting is measured to reflect the single-molecule properties, e.g., the first molecular excited state. The energy of the first excited state is typically determined by a rising position of the photon counting as a function of the bias voltage between the tip and the substrate. It remains a challenge to determine the precise rise position of the current due to the possible experimental noise. In this work, we propose an alternating current version of STML to resolve the fine structures in the photon counting measurement. The measured photon counting and the current at the long-time limit show a sinusoidal oscillation. The zero-frequency component of the current shows knee points at the precise voltage as the fraction of the detuning between the molecular gap and the DC component of bias voltage. We propose to measure the energy level with discontinuity of the first derivative of such zero-frequency component. The current method will extend the application of STML in terms of measuring molecular properties.

**Keywords:** alternating current scanning tunneling microscope, inelastic electron scattering, single-molecule electroluminescence, molecular energy levels

---

<sup>†</sup>Corresponding author: Hui Dong, Guohui Dong, E-mail: hdong@g scaep.ac.cn, 20210076@sicnu.edu.cn

# 1. Introduction

Measuring the induced luminescence in scanning tunneling microscopy (STML) is currently arising as a powerful tool to detect the single-molecular properties, such as energy levels and optical responses [1]. The technique of generating light from a metal-insulator-metal tunneling junction was discovered by Lambe and McCarthy in 1976 [2]. Then the light emission with the nearly atomic spatial resolution is reported for a scanning tunneling microscopy (STM) [3].

The origin of emitted light in STM had been controversial that whether the photon is emitted from molecules. Intuitively, the transition involving molecular states could lead to molecular luminescence as the first origin. And the energy transfer from an excited molecular state to the metal substrate may also contribute to light emission, known as the quenching process as the second origin. Berndt et al. reported spatially resolved photon emission from STM junction [4]. And high emission efficiency from molecules was guaranteed by an oxide layer which blocks such quenching process [5]. To observe the emission solely from molecules, a decoupling layer separated the molecule from the substrate is needed [6]. By virtue of the decoupling proposal, molecular luminescence was realized with different decoupling layers and various substrates. The fluorescence from individual molecule is observed for porphyrin molecules adsorbed on a thin aluminum oxide ( $\text{Al}_2\text{O}_3$ ) film covered on a metal NiAl(100) surface [7,8] and for molecules on the organic film as the decoupling layer on the metallic substrate [9–16]. The ultra-thin insulating NaCl film was shown as a good decoupling layer [17] for the observation of luminescence, e.g., for the individual pentacene [18] and  $\text{C}_{60}$  [19] molecules from a metallic substrate. The advantage of strong enhanced molecular fluorescence caused by the decoupling method [20–23] makes the sandwich structure with metallic tip, decoupling layer and the metallic substrate as a feasible platform for the STML experiments. And our current work will focus on such structure.

In general, the theory of STML includes three mechanisms, i.e., the inelastic electron scattering (IES) mechanism, the charge injection (CI) mechanism and the gap plasmon mechanism. We focus on the IES mechanism where the electron tunnels from one electrode to the other inelastically while exciting the molecule in the gap. In the sandwich setup, the tunneling current as well as the luminescence photon is detected as a function of the bias voltage applied between the tip and the substrate.

Once the energy of the tunneling electron is above a molecular transition gap, the single molecule can be pumped to an excited state and then fluoresces. Thus a rise of the photon counting can be observed at the position where the tunneling electron energy matches the molecular transition energy [24]. And the molecular energy level can be determined by the rise position of the photon counting [25]. Yet, it is difficult to accurately determine the energy level due to the possible noise in the experiments [26].

In this paper, we propose an AC-STML method to detect the fine molecular levels. Originally, STM with alternating current [27] was developed to probe the noise spectrum. Here, we extend its application in molecular structure detection. To resolve the molecular structure, we calculate the current and the luminescence photon counting for the AC bias STM with perturbation theory and express the current in the series of the Bessel's function. We find that the measured photon counting and the inelastic current oscillate with time at the long-time limit. The zero-frequency component of the Fourier transformation of the current shows knee points at the precise voltage as the fraction of the detuning between the molecular gap and the DC (time-independent) component of bias voltage. The fine molecular structure can be determined specifically with the knee points in the DC current (the zero-frequency component of the AC current) as a function of the driving AC frequency.

The rest of the paper is organized as follows. In Sec. 2 we describe our model of STML with AC bias and calculate the inelastic tunneling current in the time domain through the Bessel's function of the first kind. Then we obtain the zero-frequency current in the frequency domain. Section 3 shows the current and the first derivative of the current as a function of AC frequency. We summarize the main contributions in Section 4.

## 2. Methods

**The inelastic current in STML.** We sketch the setup of the AC-STML system in Fig. 1. The molecule is decoupled by a thin NaCl layer (the blue layer) from the metal substrate (the grey layer). Here, we describe the molecule with dipole approximation [24]. The nucleus is marked by the yellow sphere and the molecular electron is marked by the black sphere. The tip generates a tunneling electron (the red sphere) by the AC bias applied between the tip and the substrate. The AC bias  $V_b(t) = V_0 + V_1 \sin(\nu t)$  contains a time-independent part  $V_0$  and a sinusoidal part with amplitude  $V_1$

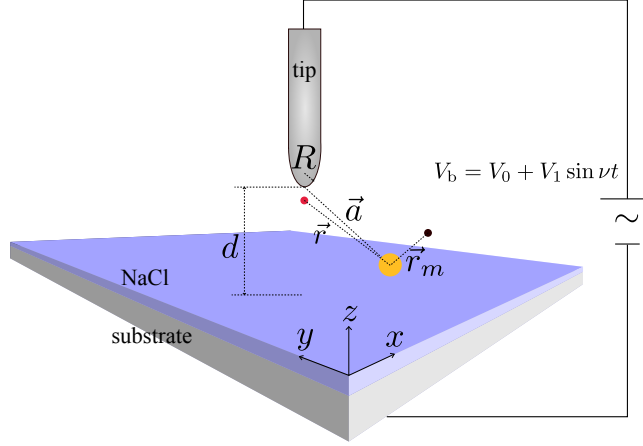


Figure 1: The schematic diagram of the AC STML system. In the dipole approximation, the yellow (black) sphere represents the molecular nucleus (molecular electron). The molecule is separated from the metallic substrate by the decoupling layer. The red sphere stands for the tunneling electron. The radius of the tip apex is  $R$ .  $d$  represents the distance between the bottom of the tip and the decoupling layer.  $\vec{r}$  ( $\vec{r}_m$ ,  $\vec{a}$ ) means the distance from the tunneling electron (molecular electron, the center of the tip's apex) to the nucleus. The AC bias  $V_b(t) = V_0 + V_1 \sin(\nu t)$  is applied between the tip and the substrate.

and frequency  $\nu$ . The radius of the tip's apex is  $R$ , and  $d$  denotes the distance from the bottom of the tip to the substrate. The molecular nucleus is set as the origin of the coordinate system.  $\vec{r}$ ,  $\vec{r}_m$  and  $\vec{a}$  denote the coordinates of the tunneling electron, the molecular electron and the center of the tip's apex, respectively. The tunneling electron interacts with the molecule via the Coulomb interaction. The molecule can be excited by the tunneling electron and subsequently emit photons via spontaneous emission.

The Hamiltonian in our AC-STML system is divided into three parts,

$$\hat{H}_{\text{total}} = \hat{H}_{\text{el}} + \hat{H}_m + \hat{H}_{\text{el-m}}, \quad (1)$$

where  $\hat{H}_{\text{el}} = -\hbar^2 \nabla^2 / 2m_e + V(\vec{r})$  corresponds to the Hamiltonian of the tunneling electron.  $m_e$  is the electron mass, and  $V(\vec{r})$  is the potential for the tunneling electron at the position  $\vec{r}$ .  $\hat{H}_m = E_g |\chi_g\rangle \langle \chi_g| + E_e |\chi_e\rangle \langle \chi_e|$  is the Hamiltonian of the molecule which is simplified as a two-level system [28–30].  $|\chi_g\rangle$  is the molecular ground state with energy  $E_g$ , and  $|\chi_e\rangle$  is the molecular excited

state with energy  $E_e$ .  $\hat{H}_{\text{el-m}} \simeq -e\hat{\boldsymbol{\mu}} \cdot \vec{r}/|\vec{r}|^3$  is the Coulomb interaction between the tunneling electron and the molecule.  $e$  is the electron charge, and  $\hat{\boldsymbol{\mu}}$  is the electric dipole moment operator of the molecule [24]. This interaction will induce the molecular transition between its two states in the inelastic tunneling process.

The electron wavefunctions in the state  $k$  of the tip and in the state  $n$  of the substrate are written [31] as

$$\langle \vec{r} | \phi_k \rangle = A_k \frac{e^{-\kappa_k(|\vec{r}-\vec{a}|-R)}}{\kappa_k |\vec{r}-\vec{a}|}, \quad (2)$$

$$\langle \vec{r} | \varphi_n \rangle = B_n e^{-\kappa_n |z|}, \quad (3)$$

where  $\kappa_k = \sqrt{-2m_e \xi_k / \hbar}$  ( $\kappa_n = \sqrt{-2m_e E_n / \hbar}$ ) characterizes the decay factor of the tunneling electron with energy  $\xi_k$  ( $E_n$ ) in the tip (substrate).  $A_k$  and  $B_n$  are the normalized coefficients derived from the first-principle calculation [32, 33].

At a given bias, both the elastic and the inelastic tunneling occur. The interaction between the molecule and the tunneling electron is small and is treated as a perturbation. Thus the probability of the molecule in its excited state is quite low [34]. At the beginning, we assume that the molecule is in its ground state and the tunneling electron is in the state  $n$  of the substrate, i.e.,  $|\Psi(0)\rangle = |\chi_g\rangle |\varphi_n\rangle$  noticing the typical low temperature in the STML experiments [7, 8, 18]. Using the time-dependent perturbation theory, we find that at time  $t$ , the system evolves to state

$$|\Psi(t)\rangle = e^{-i(E_n+E_g)t/\hbar} |\chi_g\rangle |\varphi_n\rangle + \sum_k c_{g,k}(t) |\chi_g\rangle |\phi_k\rangle + \sum_k c_{e,k}(t) |\chi_e\rangle |\phi_k\rangle, \quad (4)$$

where  $c_{g,k}(t)$  is the elastic tunneling amplitude and  $c_{e,k}(t)$  is the inelastic tunneling amplitude. The dynamical equations of the tunneling amplitudes read

$$i\hbar \frac{dc_{g,k}(t)}{dt} = \left( \tilde{\xi}_k(t) + E_g \right) c_{g,k}(t) + e^{-i(\tilde{E}_n+E_g)t/\hbar} \mathcal{M}_{n,k}, \quad (5)$$

$$i\hbar \frac{dc_{e,k}(t)}{dt} = \left( \tilde{\xi}_k(t) + E_e \right) c_{e,k}(t) + \mathcal{N}_{s,t} |_{V_b, E_n \rightarrow \xi_k} e^{-i(\tilde{E}_n+E_g)t/\hbar}, \quad (6)$$

where  $\mathcal{M}_{n,k}$  is the transition matrix element in the elastic tunneling and  $\mathcal{N}_{s,t} |_{V_b, E_n \rightarrow \xi_k}$  is the transition matrix element from the substrate's state to the tip's state under the AC bias  $V_b$  [24].  $\tilde{E}_n$  ( $\tilde{\xi}_k$ ) is the

electron energy in the substrate (tip) under the bias. In this work, we apply an AC bias  $V_b(t)$  between the electrodes. In this case, we have the simple relations,  $\tilde{\xi}_k = \xi_k + eV_0 + eV_1 \sin(\nu t)$  and  $\tilde{E}_n = E_n$ .

The inelastic tunneling rate is written as

$$\begin{aligned} \frac{d}{dt} |c_{e,k}(t)|^2 &= \frac{2}{\hbar^2} \mathcal{N}_{s,t}^2 |_{V_b, E_n \rightarrow \xi_k} \text{Re} \left\{ e^{-i \left[ Bt - \frac{eV_1}{\hbar\nu} \cos(\nu t) \right]} \right. \\ &\quad \left. \times \int_0^t d\tau e^{i \left[ B\tau - \frac{eV_1}{\hbar\nu} \cos(\nu\tau) \right]} \right\}, \end{aligned} \quad (7)$$

where we have used the notation  $B \equiv (\xi_k - E_n + E_{eg} + eV_0) / \hbar$ . The inelastic electron current is

$$I_{s,t}(t) = e \sum_{n,k} F_{\mu_0,T}(E_n) [1 - F_{\mu_0,T}(\xi_k)] \frac{d}{dt} |c_{e,k}(t)|^2, \quad (8)$$

where  $F_{\mu_0,T}(E) = 1 / \{ \exp[(E - \mu_0) / k_B T] + 1 \}$  is the Fermi-Dirac distribution of the electron in the tip or substrate at energy  $E$  and temperature  $T$ .  $k_B$  is the Boltzmann constant and  $\mu_0$  is the Fermi energy. The subscript of  $I_{s,t}$  means that the tunneling electron passes from the substrate to the tip. In experiments, STML is performed under a very low temperature, e.g., 5K or 13K [7, 8, 18]. Therefore, the Fermi-Dirac distribution is simplified as  $F_{\mu_0,T}(E) = 1$  for  $E < \mu_0$  and  $F_{\mu_0,T}(E) = 0$  for  $E \geq \mu_0$ . The inelastic current is thus rewritten as  $I_{s,t}(t) = e \sum_{n,k} \frac{d}{dt} |c_{e,k}(t)|^2$ .

By replacing the summation with integral and using Jacobi-Anger expansion  $e^{i a \cos(\nu t)} = \sum_{l=-\infty}^{\infty} e^{i l \pi / 2} J_l(a) e^{i l \nu t}$ , we obtain the inelastic tunneling current explicitly as

$$\begin{aligned} I_{s,t}(t) &= \int_{-\infty}^{\mu_0} dE_n \int_{\mu_0}^0 d\xi_k \rho_s(E_n) \rho_t(\xi_k) \frac{d}{dt} |c_{e,k}(t)|^2 \\ &= \frac{2}{\hbar^2} \int_{2\mu_0}^{\mu_0} dE_n \int_{\mu_0}^0 d\xi_k \rho_s(E_n) \rho_t(\xi_k) \\ &\quad \times \mathcal{N}_{s,t}^2 |_{V_b, E_n \rightarrow \xi_k} \sum_{l,l'=-\infty}^{\infty} (-1)^{l'} \\ &\quad \times J_l \left( \frac{eV_1}{\hbar\nu} \right) J_{l'} \left( \frac{eV_1}{\hbar\nu} \right) (B - l'\nu)^{-1} \\ &\quad \times \{ \cos[(l - l')\nu t + (l + l' - 1)\pi/2] \\ &\quad - \cos[-(B - l\nu)t + (l + l' - 1)\pi/2] \}, \end{aligned} \quad (9)$$

where  $\rho_s(E)$  ( $\rho_t(E)$ ) is the density of state in the substrate (tip) at energy  $E$ .  $E_{eg} = E_e - E_g$  is the molecular energy gap, and  $J_i(x)$  is the  $i$ -th Bessel function of the first kind. In the derivation above,

we have used the property of the Bessel functions  $J_i(-a) = (-1)^i J_i(a)$ . We change the range of the integral about  $E_n$  from  $[-\infty, \mu_0]$  to  $[2\mu_0, \mu_0]$ , since most electrons of the metal occupy states near the Fermi energy. The detailed derivations are presented in Appendix A.

**AC-current in frequency domain.** Different from DC voltage case, the system under the AC bias will not reach a steady state with a constant current at the long-time limit. Instead, the current oscillates with various Fourier frequencies. The information of the energy level can be extracted from these components in the Fourier transformations of  $I_{s,t}(t)$  as following

$$\begin{aligned}
I_{s,t}(\omega) &= \int_{-\infty}^{+\infty} dt e^{i\omega t} I_{s,t}(t) \\
&= \frac{2\pi}{\hbar^2} \int_{2\mu_0}^{\mu_0} dE_n \int_{\mu_0}^0 d\xi_k \rho_s(E_n) \rho_t(\xi_k) \\
&\quad \times \mathcal{N}_{s,t}^2 |V_b, E_n \rightarrow \xi_k| \sum_{l, l'=-\infty}^{\infty} (-1)^{l'} \\
&\quad \times J_l\left(\frac{eV_1}{\hbar v}\right) J_{l'}\left(\frac{eV_1}{\hbar v}\right) (B - l'v)^{-1} \\
&\quad \times \{ \delta[(l - l')v + \omega] e^{i(l+l'-1)\pi/2} \\
&\quad + \delta[(l - l')v - \omega] e^{-i(l+l'-1)\pi/2} \\
&\quad - \delta[(B - lv) + \omega] e^{-i(l+l'-1)\pi/2} \\
&\quad - \delta[(B - lv) - \omega] e^{i(l+l'-1)\pi/2} \}. \tag{10}
\end{aligned}$$

Here, we have used the relation  $\int_{-\infty}^{+\infty} dt e^{i\Omega t} = 2\pi\delta(\Omega)$ .

The photon counting in the AC system heavily depends on the AC inelastic tunneling current we calculated above. As the molecule is firstly excited to its excited state by the AC bias and then decays back through the spontaneous emission process, the population equation of the molecule excited state reads [24]  $\dot{P}_e(t) = -\gamma P_e(t) + I_{s,t}(t)$ , where  $P_e(t)$  stands for the excited-state population and  $\gamma$  is the spontaneous decay rate. Since the AC inelastic tunneling current oscillates with various Fourier frequencies, we divide the excited-state population  $P_e(t)$  with respect to the Fourier frequencies, i.e.,  $-i\omega P_e(\omega) = -\gamma P_e(\omega) + I_{s,t}(\omega)$  where  $P_e(\omega) = \int_{-\infty}^{\infty} P_e(t) e^{i\omega t} dt$ . Thus, the zero-component current contributes to a steady photon counting in the long-time limit while every nonzero-frequency component gives one time-dependent photon counting with its corresponding frequency.

To find the energy levels, we consider the zero-frequency component of the inelastic current (Eq. (10)), i.e.,  $\omega = 0$  as

$$\begin{aligned}
I_{s,t}(\omega = 0) &= \frac{4\pi}{\hbar^2} \int_{2E_f}^{E_f} dE_n \int_{E_f}^0 d\xi_k \rho_s(E_n) \rho_t(\xi_k) \\
&\times \mathcal{N}_{s,t}^2 |_{V_b, E_n \rightarrow \xi_k} \sum_{l, l' = -\infty}^{\infty} (-1)^{l'} \\
&\times J_l \left( \frac{eV_1}{\hbar v} \right) J_{l'} \left( \frac{eV_1}{\hbar v} \right) (B - l'v)^{-1} \\
&\times \cos \left[ (l + l' - 1) \pi / 2 \right] \\
&\times \left\{ \delta \left[ (l - l') v \right] - \delta \left( B - lv \right) \right\}. \tag{11}
\end{aligned}$$

The result shown in Eq. (11) retains the current for the case with DC voltage ( $V_1 = 0$ ) obtained in [24] by noticing  $J_0(0) = 1$  and  $J_l(0) = 0$  for any  $l \neq 0$ . In the paper [24], the current caused by the DC bias keep constant at the long-time limit, while in our AC case, the inelastic current oscillates with the time and cannot reach a steady state. So we make Fourier transformation of the AC-induced current and investigate the zero-frequency component of the current. In the long-time limit, the time-independent photon counting is proportional to the zero-component current, i.e., Eq. (11).

### 3. Results

To reveal the resonant conditions in the above current, we perform the numerical calculation of tunneling current with parameters extracted from the experimental setup. In the STML experiments, the metal used for the tip and the substrate is typically chosen as gold (Au) [35–39], silver (Ag) [1, 29, 30, 40–46] and copper (Cu) [11, 18, 47, 48]. In our simulation of the STML current, the tip and the substrate are made of silver with Fermi energy  $\mu_0 = -4.64\text{eV}$ . The calculation of the current requires the Ag's density of state, which is obtained from the book [49] by the spline interpolation of the discrete data points. The detail of the obtained density of state was presented in our previous publications [24, 50]. In the experiments, the molecular gap is typically chosen around  $1.5\text{eV} \sim 4\text{eV}$  [1, 29, 38, 42, 43, 51–53] to avoid the possible damage caused by the strong static electric field between



the tip and the substrate. For example, the energy gap between the first singlet excited state and the ground state of the free-base phthalocyanine ( $\text{H}_2\text{Pc}$ ) molecule is 1.81eV [42, 51], and the  $Q(0,0)$  transition energy of zinc-phthalocyanine ( $\text{ZnPc}$ ) molecule is 1.90eV [1, 29, 38, 43, 52, 53]. Here, we choose that the molecular gap is  $E_{\text{eg}} = 2.0\text{eV}$ . In the scanning process, the distance  $d$  between the tip and the substrate is typically around several nanometers. And we have used  $d = 0.5\text{nm}$  and the radius of the tip apex is  $R = 0.5\text{nm}$ .

**Tunneling current for the tip position  $\vec{a} = (0, 0, d)$ .** Since the absolute value of the Bessel function decreases as its order increases, it is reasonable to cut off the high order term of the Bessel function of the summation in Eq. (11). Noticing that the factor  $\cos[(l+l'-1)\pi/2]$  vanishes for the case where  $l+l'$  is even, we consider the cutoffs with  $|l-l'| \leq 3$  and  $|l-l'| \leq 5$  to check the convergence of the current in Eq. (11). Fig. 2 (a) shows the zero-frequency inelastic tunneling current as a function of AC frequency  $\nu$ . The parameters in the simulation are given as follows,  $l \in [-3, 3]$ ,  $R = 0.5\text{nm}$ ,  $d = 0.5\text{nm}$ ,  $\vec{a} = (0, 0, d)$ ,  $E_{\text{eg}} = 2\text{eV}$ ,  $eV_1/\hbar\nu = 2$ ,  $\mu_0 = -4.64\text{eV}$  and  $eV_0 = -1.88\text{eV}$ . The tip is placed right above the molecule. In Fig. 2 (a), the red dotted line reveals the current including the summation of  $|l| \leq 3$  and  $|l-l'| \leq 3$ , and the black line shows that of  $|l| \leq 3$  and  $|l-l'| \leq 5$ . The coincidence of two curves demonstrates that the zero-frequency inelastic current already converges with  $|l-l'| = 3$  and  $|l| \leq 3$ . Therefore, we use the cutoff  $|l| \leq 3$  and  $|l-l'| \leq 3$  in the following calculation.

The curve in Fig. 2 (a) also shows the discrete knee points. We numerically calculate the first derivative of the inelastic tunneling current  $I_{s,t}(\omega = 0)$  with respect to the AC frequency  $\nu$  and plot the result in Fig. 2 (b). In Fig. 2 (b), the line reveals the discontinuity of the first derivative of the zero-frequency current with the discontinuous spots located at  $\hbar\nu = 0.04\text{eV}$ ,  $0.06\text{eV}$ , and  $0.12\text{eV}$ . By defining the detuning  $\Delta = E_{\text{eg}} + eV_0$ , we find that the discontinuous spots are in agree with the condition  $\Delta - l'\hbar\nu = 0$  with  $l' = 3, 2, 1$ , respectively. Mathematically, such discontinuous behavior can be understood with Jacobi-Anger expansion. The STML system with AC bias  $V_0 + V_1 \sin(\nu t)$  is equivalent to the system with a series of DC bias  $V_l^{\text{eff}} = V_0 - l'\hbar\nu/e$  ( $l' = 0, \pm 1, \pm 2, \dots$ ). Once one effective bias  $V_l^{\text{eff}}$  matches the molecular energy gap, namely  $V_l^{\text{eff}} = E_{\text{eg}}$ , a new contribution to the molecular excitation rate (the inelastic current) emerges and results in one discontinuous point in its

first derivative curve. Therefore we have demonstrated that the discontinuous spots reveal the fine detail of the molecule.

To investigate the influence caused by the height of the tip, we choose the parameter  $d = 0.3\text{nm}$ ,  $d = 0.4\text{nm}$  and  $d = 0.5\text{nm}$  respectively. Fig. 3 (a) shows the zero-frequency component of the inelastic current which is depend on the position of the tip. The green, yellow and red curves correspond to the inelastic current with the tip fixed at  $d = 0.3\text{nm}$ ,  $d = 0.4\text{nm}$  and  $d = 0.5\text{nm}$  respectively. The inelastic current becomes larger as the tip moves to the molecule. Because we modeled the electron wavefunction of the tip as Eq.( 2), which decays with the tip radius exponentially. When the STM tip approaches the substrate, the electron wavefunction at the position of the tunneling electron increases, resulting in the increase of the transition matrix element. Finally, the inelastic current increases. Fig. 3 (b) reveals the first derivative of the inelastic current with respect to the frequency. The discontinuous data are marked by the dot. All the curves have the discontinuous data at the same spots  $\hbar\nu = 0.04\text{eV}$ ,  $0.06\text{eV}$ , and  $0.12\text{eV}$ , which are in agree with the condition  $\Delta - l'\hbar\nu = 0$ . Although the inelastic current changes with the tip approaching the molecule, the knee points of the current satisfy the resonant condition which is independent on the position of the tip.

The advantage of our AC-STML is that the frequency can be tuned with precision. In the DC bias case, the inelastic tunneling current has a sudden rise from zero when the absolute value of the DC bias equals to a critical quantity, i.e., the absolute value of the molecular energy gap divided by the electron charge [24]. And one can extract the information of the molecular energy gap from this curve theoretically. However, due to the noise of the experiment, the inelastic tunneling current curve changes smoothly near the critical quantity. Thus one can only read out the energy gap roughly. In the AC STML method, the point of the energy gap is featured as the knee point of the zero-frequency component of the AC current. These points show discontinuous and non-analytical property at the non-zero point of the current curve. By numerically calculating the first derivative of the zero-frequency component of the inelastic tunneling current with respect to the AC frequency, the discontinuous points, i.e., the sudden rising points, correspond to the points of energy resonance. We can read out discontinuous points directly and then obtain the energy gap of the molecule.

The method of realizing our proposal includes two steps. Firstly, the molecule is probed via DC bias. The molecular energy gap can be roughly obtained through the rising point in the photon-

emission spectrum. And we estimate the rough value as  $V_0$ . Secondly, we add a nonzero AC component to this DC voltage and apply this time-dependent bias to the molecule. A series of knee points can be shown in the figure of the zero-frequency inelastic tunneling current  $I_{s,t}(\omega = 0)$  as a function of AC frequency. Then, we can precisely determine these non-analytical points through the first derivative of the inelastic tunneling current  $I_{s,t}(\omega = 0)$  with respect to the AC frequency. The precise molecular gap is given with the relation  $E_{\text{cg}} - e|V_0| = l'\hbar\nu$  ( $l' = 0, \pm 1, \pm 2, \pm 3$ ).

**Tunneling current for the tip position  $\vec{a} = (0.2\text{nm}, 0, d)$ .** Without loss of generality, we consider the case where the tip is laterally displaced from the center of the molecule, e.g.,  $\vec{a} = (0.2\text{nm}, 0, d)$ . We calculate the zero-frequency inelastic current as shown in Fig. 4 (a). The curve shows the same feature as that in Fig. 2 (a). The other parameters in Fig. 4 are the same as that in Fig. 2. The coincidence between the red dotted line and the blue dashed line also shows the convergence of our calculation when we consider the summation with terms  $|l| \leq 3$  and  $|l - l'| \leq 3$ . We also calculate the first derivative of the zero-frequency inelastic current with respect to the AC frequency to explore the fine details of current. As shown in Fig. 4 (b), the first derivative of the zero-frequency inelastic current reveals the discontinuity at the same spots  $\hbar\nu = 0.04\text{eV}$ ,  $0.06\text{eV}$ , and  $0.12\text{eV}$ . The results in  $\vec{a} = (0, 0, d)$  and  $\vec{a} = (0.2\text{nm}, 0, d)$  indicate that the fine structure in the AC current is robust with respect to the relative position between the tip and molecule.

To investigate the influence of the relative position of the tip and the molecule on the inelastic current, we calculated the zero-frequency component of the current and its first derivative with respect to the frequency as a function of the frequency in Fig. 5. Since we assume that the molecular dipole is isotropic in three axes, the inelastic current is symmetric around the z-axis. Hence, we only calculate the displacement of the tip in the x-axis. In Fig. 5, the red, blue and yellow curves correspond to the cases with  $\vec{a} = (0, 0, d)$ ,  $\vec{a} = (0.1\text{nm}, 0, d)$  and  $\vec{a} = (0.2\text{nm}, 0, d)$  respectively. In Fig. 5 (a), when the tip is right above the molecule, the zero-frequency inelastic current is much smaller than the other cases. The current with  $\vec{a} = (0.1\text{nm}, 0, d)$  is a little smaller than the current with  $\vec{a} = (0.2\text{nm}, 0, d)$ . So, the inelastic current can change with the distance between the tip and the molecule. In Fig. 5 (b), the dotted markers reveal the knee points of the current at same spots  $\hbar\nu = 0.04\text{eV}$ ,  $0.06\text{eV}$ , and  $0.12\text{eV}$ , showing that the resonant relation is independent on the relative of the tip and the molecule.

To show the general case, we calculate the inelastic tunneling current and its first derivative with different energy detuning  $\Delta = 0.04, 0.06, 0.08, 0.1, \text{ and } 0.12\text{eV}$ , as illustrated in Fig. 6. The left column represents the current curves with an upward trend as discussed before. When the frequency  $\nu$  of the bias is small, the energy of the tunneling electron is too weak to excite the molecule. No inelastic tunneling electron transfers energy to the molecule and no inelastic current flows through the electrodes. The energy of the rising point in the current becomes higher as  $\Delta$  increases. From the definition  $\Delta = E_{\text{eg}} + eV_0$ , the increase of  $V_0$  causes the effective bias  $l'\hbar\nu/e - V_0$  decreasing. To reach the molecular excitation energy, the value of  $\hbar\nu$  should be larger. The right column in the Fig. 6 plots the first derivative of the current. The round (square, triangle) spot reveals the non-analysis feature of the current. With  $\Delta$  increasing, the energy of the knee point in the same shape increases too.

To figure out the relation between the energy of knee points and  $\Delta$ , we show the energy of knee points as the function of the energy  $\Delta$  with various orders. Fig. 7 plots the energy of spots with the same markers in Fig. 6. The energy of the knee points linearly increases with energy  $\Delta$ . The slope of the line with triangle (square, round) marker is 1 (1/2, 1/3), and matches  $1/l'$  in the relation  $\Delta - l'\hbar\nu = 0$  with  $l' = 1 (2, 3)$ . This demonstrates that the molecular gap  $E_{\text{eg}}$  can be determined via the knee points  $\Delta - l'\hbar\nu = 0$ .

## 4. Conclusions

In summary, we have proposed the AC-STML setup to measure fine molecular structures. We calculate the photon counting reflected by the inelastic current and obtain its Fourier components at the long-time limit. We show that the rising position of the current spectrum is precisely determined by the match between the effective bias and the molecular energy gap. These rising positions are utilized to find the molecular energy levels by scanning the frequency of the AC bias. The observations here allow us to propose an alternative method to determine the molecular levels, especially the fine structures around electronic levels, e.g., the vibrational levels.

The AC-STML method can be realized in experiments. Theoretically, our proposal works well in a large range of AC frequency. In reality, the AC frequency can be realized around GHz [54]. Therefore, as long as we can localize the rough bias  $V_0$  to the range  $|E_{\text{eg}} - e|V_0| \leq 10\mu\text{eV}$  through

the inelastic current curve in the DC bias case, the precise energy gap will be obtained successfully.

## Acknowledgements

This work is supported by the National Natural Science Foundation of China (NSFC) (Grant No. 11875049), the NSAF (Grant Nos. U1730449 and U1930403), and the National Basic Research Program of China (Grant No. 2016YFA0301201).

## Appendix A . The derivation of the AC current

The first derivative of the inelastic tunneling amplitude  $c_{e,k}(t)$

$$\begin{aligned} i\hbar \frac{dc_{e,k}(t)}{dt} &= \left( \tilde{\xi}_k(t) + E_e \right) c_{e,k}(t) \\ &+ \mathcal{N}_{s,t}|_{V_b, E_n \rightarrow \xi_k} e^{-i(\tilde{E}_n + E_g) \frac{t}{\hbar}}. \end{aligned}$$

By using the relation  $\tilde{\xi}_k = \xi_k + eV_0 + eV_1 \sin(vt)$  and  $\tilde{E}_n = E_n$ , we rewrite the inelastic tunneling amplitude  $c_{e,k}(t)$  as

$$\begin{aligned} \frac{dc_{e,k}(t)}{dt} &= \frac{1}{i\hbar} [\xi_k + eV_0 + eV_1 \sin(vt) + E_e] c_{e,k}(t) \\ &+ \frac{1}{i\hbar} \mathcal{N}_{s,t}|_{V_b, E_n \rightarrow \xi_k} e^{-i(E_n + E_g) \frac{t}{\hbar}}. \end{aligned}$$

The solution of the inelastic tunneling amplitude  $c_{e,k}(t)$  is

$$\begin{aligned} c_{e,k}(t) &= \frac{1}{i\hbar} \mathcal{N}_{s,t}|_{V_b, E_n \rightarrow \xi_k} e^{-i \left[ (\xi_k + E_e + eV_0) \frac{t}{\hbar} - \frac{eV_1}{\hbar v} \cos(vt) \right]} \\ &\times \int_0^t d\tau e^{i \left[ (\xi_k - E_n + E_{eg} + eV_0) \frac{\tau}{\hbar} - \frac{eV_1}{\hbar v} \cos(v\tau) \right]}. \end{aligned}$$

The inelastic tunneling rate can be expressed as

$$\begin{aligned}
\frac{d|c_{e,k}(t)|^2}{dt} &= \frac{d}{dt} [c_{e,k}(t) \cdot c_{e,k}^*(t)] \\
&= \frac{dc_{e,k}^*(t)}{dt} \cdot c_{e,k}(t) + c.c \\
&= \left\{ -\frac{1}{i\hbar} [\xi_k + eV_0 + eV_1 \sin(vt) + E_e] c_{e,k}^*(t) \right. \\
&\quad \left. - \frac{1}{i\hbar} \mathcal{N}_{s,t}^* |_{V_b, E_n \rightarrow \xi_k} e^{i(E_n + E_g) \frac{t}{\hbar}} \right\} \cdot c_{e,k}(t) + c.c \\
&= -\frac{1}{i\hbar} \mathcal{N}_{s,t}^* |_{V_b, E_n \rightarrow \xi_k} e^{i(E_n + E_g) \frac{t}{\hbar}} c_{e,k}(t) + c.c.
\end{aligned}$$

Substituting the inelastic tunneling amplitude  $c_{e,k}(t)$  into the inelastic tunneling rate  $d|c_{e,k}(t)|^2/dt$ , we have

$$\begin{aligned}
\frac{d|c_{e,k}(t)|^2}{dt} &= \frac{1}{\hbar^2} \mathcal{N}_{s,t}^2 |_{V_b, E_n \rightarrow \xi_k} e^{i(E_n + E_g) \frac{t}{\hbar}} \\
&\quad \times e^{-i\left[\left(\xi_k + E_e + eV_0\right) \frac{t}{\hbar} - \frac{eV_1}{\hbar v} \cos(vt)\right]} \\
&\quad \times \int_0^t d\tau e^{i\left[\left(\xi_k - E_n + E_{eg} + eV_0\right) \frac{\tau}{\hbar} - \frac{eV_1}{\hbar v} \cos(v\tau)\right]} + c.c \\
&= \frac{1}{\hbar^2} \mathcal{N}_{s,t}^2 |_{V_b, E_n \rightarrow \xi_k} \\
&\quad \times e^{-i\left[\left(\xi_k + E_{eg} + eV_0 - E_n\right) \frac{t}{\hbar} - \frac{eV_1}{\hbar v} \cos(vt)\right]} \\
&\quad \times \int_0^t d\tau e^{i\left[\left(\xi_k - E_n + E_{eg} + eV_0\right) \frac{\tau}{\hbar} - \frac{eV_1}{\hbar v} \cos(v\tau)\right]} + c.c. \tag{12}
\end{aligned}$$

Then Eq. (12) can be rewritten as

$$\begin{aligned}
\frac{d|c_{e,k}(t)|^2}{dt} &= \frac{1}{\hbar^2} \mathcal{N}_{s,t}^2 |_{V_b, E_n \rightarrow \xi_k} e^{-i\left[Bt - \frac{eV_1}{\hbar v} \cos(vt)\right]} \\
&\quad \times \int_0^t d\tau e^{i\left[B\tau - \frac{eV_1}{\hbar v} \cos(v\tau)\right]} + c.c \\
&= \frac{2}{\hbar^2} \mathcal{N}_{s,t}^2 |_{V_b, E_n \rightarrow \xi_k} \operatorname{Re} \left\{ e^{-i\left[Bt - \frac{eV_1}{\hbar v} \cos(vt)\right]} \right. \\
&\quad \left. \times \int_0^t d\tau e^{i\left[B\tau - \frac{eV_1}{\hbar v} \cos(v\tau)\right]} \right\},
\end{aligned}$$

where we have defined the notation  $B \equiv (\xi_k - E_n + E_{eg} + eV_0) / \hbar$ .

Using the Jacobi-Anger expansion  $e^{ia\cos(vt)} = \sum_{l=-\infty}^{\infty} e^{il\pi/2} J_l(a) e^{ilvt}$  we have

$$\begin{aligned}
e^{i\frac{eV_1}{\hbar v} \cos(vt)} &= \sum_{l=-\infty}^{\infty} e^{il\pi/2} J_l\left(\frac{eV_1}{\hbar v}\right) e^{ilvt}, \\
e^{-i\frac{eV_1}{\hbar v} \cos(vt)} &= e^{-i\frac{eV_1}{\hbar v} \cos(-vt)} \\
&= \sum_{l=-\infty}^{\infty} e^{il\pi/2} J_l\left(-\frac{eV_1}{\hbar v}\right) e^{-ilvt}.
\end{aligned}$$

The inelastic tunneling rate can be expressed through the series of Bessel's function

$$\begin{aligned}
\frac{d|c_{e,k}(t)|^2}{dt} &= \frac{2}{\hbar^2} \mathcal{N}_{s,t}^2 |V_b, E_n \rightarrow \xi_k| \\
&\quad \sum_{l,l'=-\infty}^{\infty} \operatorname{Re} \left\{ e^{-iBt} e^{il\pi/2} J_l\left(\frac{eV_1}{\hbar v}\right) e^{ilvt} \right. \\
&\quad \times \left. \int_0^t d\tau e^{iB\tau} e^{il'\pi/2} J_{l'}\left(-\frac{eV_1}{\hbar v}\right) e^{-il'\nu\tau} \right\} \\
&= \frac{2}{\hbar^2} \mathcal{N}_{s,t}^2 |V_b, E_n \rightarrow \xi_k| \\
&\quad \times \sum_{l,l'=-\infty}^{\infty} (-1)^{l'} J_l\left(\frac{eV_1}{\hbar v}\right) J_{l'}\left(\frac{eV_1}{\hbar v}\right) \\
&\quad \times \operatorname{Re} \left\{ e^{-i(B-l\nu)t} e^{i(l+l')\pi/2} \int_0^t d\tau e^{i(B-l'\nu)\tau} \right\}, \tag{13}
\end{aligned}$$

where we have used the relation  $J_l(-a) = (-1)^l J_l(a)$ . Calculating the integral, we obtain

$$\begin{aligned}
\frac{d|c_{e,k}(t)|^2}{dt} &= \frac{2}{\hbar^2} \mathcal{N}_{s,t}^2 |_{V_b, E_n \rightarrow \xi_k} \sum_{l, l' = -\infty}^{\infty} (-1)^{l'} \\
&\times J_l\left(\frac{eV_1}{\hbar v}\right) J_{l'}\left(\frac{eV_1}{\hbar v}\right) (B - l'v)^{-1} \\
&\times \text{Re} \left\{ e^{i[(l-l')vt + (l+l'-1)\pi/2]} \right. \\
&\quad \left. - e^{i[-(B-lv)t + (l+l'-1)\pi/2]} \right\} \\
&= \frac{2}{\hbar^2} \mathcal{N}_{s,t}^2 |_{V_b, E_n \rightarrow \xi_k} \sum_{l, l' = -\infty}^{\infty} (-1)^{l'} \\
&\times J_l\left(\frac{eV_1}{\hbar v}\right) J_{l'}\left(\frac{eV_1}{\hbar v}\right) (B - l'v)^{-1} \\
&\times \left\{ \cos[(l-l')vt + (l+l'-1)\pi/2] \right. \\
&\quad \left. - \cos[-(B-lv)t + (l+l'-1)\pi/2] \right\}. \tag{14}
\end{aligned}$$

The inelastic current is  $I_{s,t}(t) = e \sum_{n,k} \frac{d}{dt} |c_{e,k}(t)|^2$ .

By replacing the summation with integral and substituting the inelastic tunneling rate Eq. (14) into the current above  $I_{s,t}(t)$ , we obtain the inelastic tunneling current explicitly as (Eq. (9) in the main text)

$$\begin{aligned}
I_{s,t}(t) &= \int_{-\infty}^{\mu_0} dE_n \int_{\mu_0}^0 d\xi_k \rho_s(E_n) \rho_t(\xi_k) \frac{d}{dt} |c_{e,k}(t)|^2 \\
&= \frac{2}{\hbar^2} \int_{2\mu_0}^{\mu_0} dE_n \int_{\mu_0}^0 d\xi_k \rho_s(E_n) \rho_t(\xi_k) \\
&\times \mathcal{N}_{s,t}^2 |_{V_b, E_n \rightarrow \xi_k} \sum_{l, l' = -\infty}^{\infty} (-1)^{l'} \\
&\times J_l\left(\frac{eV_1}{\hbar v}\right) J_{l'}\left(\frac{eV_1}{\hbar v}\right) (B - l'v)^{-1} \\
&\times \left\{ \cos[(l-l')vt + (l+l'-1)\pi/2] \right. \\
&\quad \left. - \cos[-(B-lv)t + (l+l'-1)\pi/2] \right\}. \tag{15}
\end{aligned}$$



## References

- [1] Zhang L, Yu Y J, Chen L G, Luo Y, Yang B, Kong F F, Chen G, Zhang Y, Zhang Q, Luo Y, Yang J L, Dong Z C and Hou J G 2017 Electrically driven single-photon emission from an isolated single molecule *Nat Commun* **8**, 133.
- [2] Lambe J and McCarthy S L 1976 Light emission from inelastic electron tunneling *Phys. Rev. Lett.* **37** 923–925 1.
- [3] Coombs J H, Gimzewski J K, Reihl B, Sass J K and Schlittler R R 1988 Photon emission experiments with the scanning tunnelling microscope *J. Microsc.* **152** 325–336 1.
- [4] Berndt R, Gaisch R, Gimzewski J K, Reihl B, Schlittler R R, Schneider W D and Tschudy M 1993 Photon emission at molecular resolution induced by a scanning tunneling microscope *Science* **262** 1425–1427 1.
- [5] Flaxer E, Sneh O and Cheshnovsky O 1993 Molecular light emission induced by inelastic electron tunneling *Science* **262** 2012–2014 1.
- [6] Hoffmann G, Libiouille L and Berndt R 2002 Tunneling-induced luminescence from adsorbed organic molecules with submolecular lateral resolution *Phys. Rev. B* **65** 212107 1.
- [7] Qiu X H 2003 Vibrationally resolved fluorescence excited with submolecular precision *Science* **299** 542–546, 12.
- [8] Qiu X H, Nazin G V and Ho W 2004 Vibronic states in single molecule electron transport *Phys. Rev. Lett.* **92** 206102, 12.
- [9] Dong Z C, Guo X L, Trifonov A S, Dorozhkin P S, Miki K, Kimura K, Yokoyama S and Mashiko S 2004 Vibrationally resolved fluorescence from organic molecules near metal surfaces in a scanning tunneling microscope *Phys. Rev. Lett.* **92** 086801 1.
- [10] Guo X L, Dong Z C, Trifonov A S, Yokoyama S, Mashiko S and Okamoto T 2004 Tunneling-electron-induced molecular luminescence from a nanoscale layer of organic molecules on metal substrates *Appl. Phys. Lett.* **84** 969–971 1.
- [11] Guo X L, Dong Z C, Trifonov A, Miki K, Kimura K and Mashiko S 2005 STM-induced light emission from the surface of H2TBP porphyrin/PFP porphyrin/Cu(100) *Appl. Surf. Sci.* **241** 28–32, B.
- [12] Guo X, Dong Z, Trifonov A, Miki K, Kimura K and Mashiko S 2005 STM-induced molecular fluorescence from porphyrin molecules on metal substrates *Appl. Phys. A* **81** 367–370 1.
- [13] Liu H W, Ie Y, Nishitani R, Aso Y and Iwasaki H 2007 Bias dependence of tunneling-electron-induced molecular fluorescence from porphyrin films on noble-metal substrates *Phys. Rev. B* **75** 115429 1.
- [14] Liu H, Yan L and Iwasaki H 2007 STM-excited molecular fluorescence from MEH-PPV conjugated polymer on Ag and Au *Chem. Phys. Lett.* **450** 101–106 1.
- [15] Liu H, Ie Y, Nishitani R, Han T, Aso Y and Iwasaki H 2008 Substrate effect of STM-induced luminescence from porphyrin molecules *Thin Solid Films* **516** 2727–2730 1.
- [16] Ino D, Yamada T and Kawai M 2008 Luminescence from 3,4,9,10-perylene-tetracarboxylic dianhydride on Ag(111) surface excited by tunneling electrons in scanning tunneling microscopy *J. Chem. Phys.* **129** 014701 1.
- [17] Guo J, Lv J T, Feng Y, Chen J, Peng J, Lin Z, Meng X, Wang Z, Li X Z, Wang E G and Jiang Y 2016 Nuclear quantum effects of hydrogen bonds probed by tip-enhanced inelastic electron tunneling *Science* **352** 321–325 1.
- [18] Repp J, Meyer G, Stojković S M, Gourdon A and Joachim C 2005 Molecules on insulating films: Scanning-tunneling microscopy imaging of individual molecular orbitals *Phys. Rev. Lett.* **94** 026803, 12, 2.
- [19] Čavar E, Blüm M C, Pivetta M, Patthey F, Chergui M and Schneider W D 2005 Fluorescence and phosphorescence from individual C60 molecules excited by local electron tunneling [10.1016/j.tsf.2007.04.068](https://doi.org/10.1016/j.tsf.2007.04.068) *Phys. Rev. Lett.* **95** 196102 1.

- [20] Liu H, Ie Y, Yoshinobu T, Aso Y, Iwasaki H and Nishitani R 2006 Plasmon-enhanced molecular fluorescence from an organic film in a tunnel junction *Appl. Phys. Lett.* **88** 061901 1.
- [21] Liu H W, Nishitani R, Han T Z, Ie Y, Aso Y and Iwasaki H 2009 STM fluorescence of porphyrin enhanced by a strong plasmonic field and its nanoscale confinement in an STM cavity *Phys. Rev. B* **79** 125415 1.
- [22] Yan L, Liu H and Iwasaki H 2007 Mutual enhancement between plasmon and molecular fluorescence of conjugated polymer on metal substrates induced by STM *Chem. Phys. Lett.* **433** 312–316 1.
- [23] You S, Lv J T, Guo J and Jiang Y 2017 Recent advances in inelastic electron tunneling spectroscopy *Advances in Physics: X* **2** 907–936 1.
- [24] Dong G, You Y and Dong H 2020 Microscopic origin of molecule excitation via inelastic electron scattering in scanning tunneling microscope *New J. Phys.* **22** 113010, ~~113010~~.
- [25] Du W, Wang T, Chu H S, Wu L, Liu R, Sun S, Phua W K, Wang L, Tomczak N and Nijhuis C A 2016 On-chip molecular electronic plasmon sources based on self-assembled monolayer tunnel junctions *Nat. Photonics* **10** 274–280 1.
- [26] Imada H, Imai-Imada M, Miwa K, Yamane H, Iwasa T, Tanaka Y, Toriumi N, Kimura K, Yokoshi N, Muranaka A, Uchiyama M, Taketsugu T, Kato Y K, Ishihara H and Kim Y 2021 Single-molecule laser nanospectroscopy with micro-electron volt energy resolution *Science* **373** 95–98 1.
- [27] Guyon R, Jonckheere T, Mujica V, Crépieux A and Martin T 2005 Current and noise in a model of an alternating current scanning tunneling microscope molecule-metal junction *J. Chem. Phys.* **122** 144703 1.
- [28] Nian L L, Wang Y and Lv J T 2018 On the fano line shape of single molecule electroluminescence induced by a scanning tunneling microscope *Nano Lett.* **18** 6826–6831 2.
- [29] Zhang Y, Luo Y, Zhang Y, Yu Y J, Kuang Y M, Zhang L, Meng Q S, Luo Y, Yang J L, Dong Z C and Hou J G 2016 Visualizing coherent intermolecular dipole-dipole coupling in real space *Nature* **531** 623–627, ~~23~~.
- [30] Chen G, Luo Y, Gao H, Jiang J, Yu Y, Zhang L, Zhang Y, Li X, Zhang Z and Dong Z 2019 Spin-triplet-mediated up-conversion and crossover behavior in single-molecule electroluminescence *Phys. Rev. Lett.* **122** 177401, ~~2~~.
- [31] Bardeen J 1961 Tunnelling from a many-particle point of view *Phys. Rev. Lett.* **6** 57–59 2.
- [32] Tersoff J and Hamann D R 1983 Theory and application for the scanning tunneling microscope *Phys. Rev. Lett.* **50** 1998–2001 2.
- [33] Tersoff J and Hamann D R 1985 Theory of the scanning tunneling microscope *Phys. Rev. B* **31** 805–813 2.
- [34] Chong M 2021 *Electrically driven fluorescence of single molecule junctions* Ph.D. thesis Université de Strasbourg 2.
- [35] Chong M C, Reecht G, Bulou H, Boeglin A, Scheurer F, Mathevet F and Schull G 2016 Narrow-line single-molecule transducer between electronic circuits and surface plasmons *Phys. Rev. Lett.* **116** 036802 3.
- [36] Große C, Merino P, Rosławska A, Gunnarsson O, Kuhnke K and Kern K 2017 Submolecular electroluminescence mapping of organic semiconductors *ACS Nano* **11** 1230–1237 3.
- [37] Merino P, Rosławska A, Leon C C, Grewal A, Große C, González C, Kuhnke K and Kern K 2018 A single hydrogen molecule as an intensity chopper in an electrically driven plasmonic nanocavity *Nano Lett.* **19** 235–241 3.
- [38] Doppagne B, Chong M C, Bulou H, Boeglin A, Scheurer F and Schull G 2018 Electrofluorochromism at the single-molecule level *Science* **361** 251–255, ~~33~~.
- [39] Rosławska A, Merino P, Große C, Leon C C, Gunnarsson O, Etzkorn M, Kuhnke K and Kern K 2018 Single charge and exciton dynamics probed by molecular-scale-induced electroluminescence *Nano Lett.* **18** 4001–4007 3.

- [40] Zhang R, Zhang Y, Dong Z C, Jiang S, Zhang C, Chen L G, Zhang L, Liao Y, Aizpurua J, Luo Y, Yang J L and Hou J G 2013 Chemical mapping of a single molecule by plasmon-enhanced raman scattering *Nature* **498** 82–86 3.
- [41] Imada H, Miwa K, Imai-Imada M, Kawahara S, Kimura K and Kim Y 2016 Real-space investigation of energy transfer in heterogeneous molecular dimers *Nature* **538** 364–367 3.
- [42] Imada H, Miwa K, Imai-Imada M, Kawahara S, Kimura K and Kim Y 2017 Single-molecule investigation of energy dynamics in a coupled plasmon-exciton system *Phys. Rev. Lett.* **119** 013901, 3.
- [43] Zhang Y, Meng Q S, Zhang L, Luo Y, Yu Y J, Yang B, Zhang Y, Esteban R, Aizpurua J, Luo Y, Yang J L, Dong Z C and Hou J G 2017 Sub-nanometre control of the coherent interaction between a single molecule and a plasmonic nanocavity *Nat Commun* **8**, 3.
- [44] Kimura K, Miwa K, Imada H, Imai-Imada M, Kawahara S, Takeya J, Kawai M, Galperin M and Kim Y 2019 Selective triplet exciton formation in a single molecule *Nature* **570** 210–213 3.
- [45] Yang B, Chen G, Ghafoor A, Zhang Y, Zhang Y, Zhang Y, Luo Y, Yang J, Sandoghdar V, Aizpurua J, Dong Z and Hou J G 2020 Sub-nanometre resolution in single-molecule photoluminescence imaging *Nat. Photonics* **14** 693–699 3.
- [46] Zoh I, Imai-Imada M, Bae J, Imada H, Tsuchiya Y, Adachi C and Kim Y 2021 Visualization of frontier molecular orbital separation of a single thermally activated delayed fluorescence emitter by STM *The Journal of Physical Chemistry Letters* **12** 7512–7518 3.
- [47] Schneider N L, L   J T, Brandbyge M and Berndt R 2012 Light emission probing quantum shot noise and charge fluctuations at a biased molecular junction *Phys. Rev. Lett.* **109** 186601 3.
- [48] Edelmann K, Wilmes L, Rai V, Gerhard L, Yang L, Wegener M, Rep  n T, Rockstuhl C and Wulfhekel W 2020 Influence of co bilayers and trilayers on the plasmon-driven light emission from cu(111) in a scanning tunneling microscope *Phys. Rev. B* **101** 205405 3.
- [49] Papaconstantopoulos D A 2015 *Handbook of the Band Structure of Elemental Solids: From Z = 1 To Z = 112* (Springer US) ISBN 978-1-4419-8264-3 URL [https://www.ebook.de/de/product/23290181/dimitris\\_a\\_papaconstantopoulos\\_handbook\\_of\\_the\\_ba](https://www.ebook.de/de/product/23290181/dimitris_a_papaconstantopoulos_handbook_of_the_ba) 3.
- [50] Dong G, Hu Z, Sun X and Dong H 2021 Structural reconstruction of optically invisible state in a single molecule via scanning tunneling microscope *The Journal of Physical Chemistry Letters* **12** 10034–10039 3.
- [51] Meng Q, Zhang C, Zhang Y, Zhang Y, Liao Y and Dong Z 2015 Tunneling electron induced molecular electroluminescence from individual porphyrin j-aggregates *Appl. Phys. Lett.* **107** 043103, 3.
- [52] Doppagne B, Chong M C, Lorchat E, Berciaud S, Romeo M, Bulou H, Boeglin A, Scheurer F and Schull G 2017 Vibronic spectroscopy with submolecular resolution from STM-induced electroluminescence *Phys. Rev. Lett.* **118** 127401, 3.
- [53] Dole  al J, Merino P, Redondo J, Ondi   L, Cahl  k A and   vec M 2019 Charge carrier injection electroluminescence with CO-functionalized tips on single molecular emitters *Nano Lett.* **19** 8605–8611, 3.
- [54] Gabelli J and Reulet B 2008 Dynamics of quantum noise in a tunnel junction under ac excitation *Phys. Rev. Lett.* **100** 026601 4.

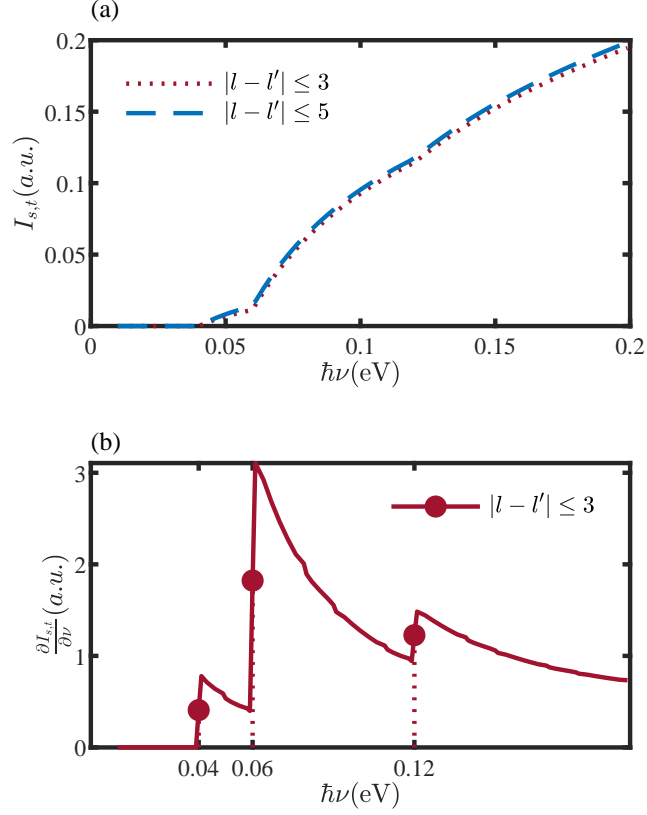


Figure 2: (a) The convergency of the zero-frequency inelastic current with  $\vec{a} = (0, 0, d)$ . The red dotted (blue dashed) curve shows the current under the summation of  $|l| \leq 3$  and  $|l - l'| \leq 3$  ( $|l - l'| \leq 5$ ). Both lines show the non-analyticity of the current with respect to the oscillating frequency. (b) The first derivative of the zero-frequency inelastic current with respect to the oscillating frequency  $\nu$ . The tip is placed right above the molecule. The red dots show the discontinuous data in the current, which correspond to  $\hbar\nu = 0.04, 0.06$ , and  $0.12\text{eV}$ . We have chosen the parameters as  $l \in [-3, 3]$ ,  $R = 0.5\text{nm}$ ,  $d = 0.5\text{nm}$ ,  $\vec{a} = (0, 0, d)$ ,  $E_{\text{eg}} = 2\text{eV}$ ,  $\mu_0 = -4.64\text{eV}$ , and  $eV_0 = -1.88\text{eV}$ . The ratio of the time-dependent voltage amplitude over the oscillating frequency is fixed at  $eV_1/\hbar\nu = 2$ .

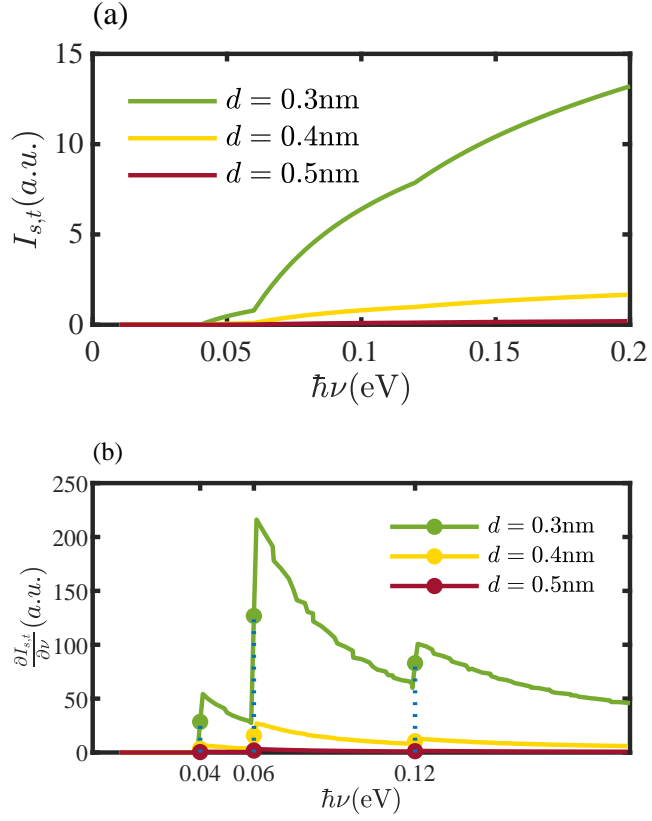


Figure 3: (a) The zero-frequency component of the inelastic current with different height of the tip. The green, yellow and red curves correspond to the inelastic current with  $d = 0.3\text{nm}$ ,  $d = 0.4\text{nm}$  and  $d = 0.5\text{nm}$  respectively. (b) The first derivative of the zero-frequency inelastic current with respect to the frequency  $\nu$ . The tip is placed right above the molecule. The dotted markers in (b) show the discontinuous data at  $\hbar\nu = 0.04\text{eV}$ ,  $0.06\text{eV}$ , and  $0.12\text{eV}$ . The other parameters are the same as before.

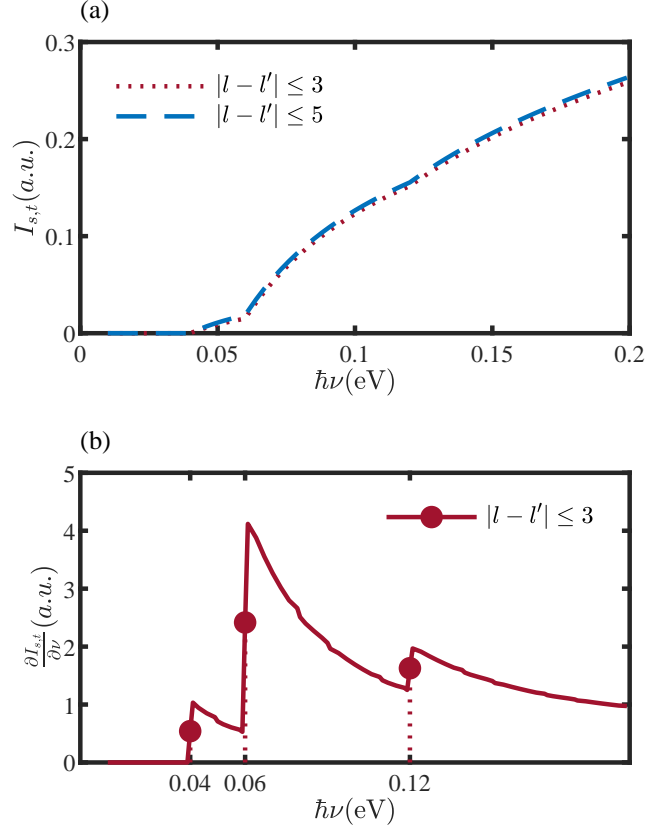


Figure 4: (a) The convergency of the zero-frequency inelastic current in  $\vec{a} = (0.2\text{nm}, 0, d)$ . The red dotted line and the blue dashed line correspond to the condition  $|l-l'| \leq 3$  and  $|l-l'| \leq 5$ , respectively. (b) The first-order derivative of the zero-frequency inelastic current about the bias frequency  $\nu$  in  $\vec{a} = (0.2\text{nm}, 0, d)$ . The other parameters are the same as before.

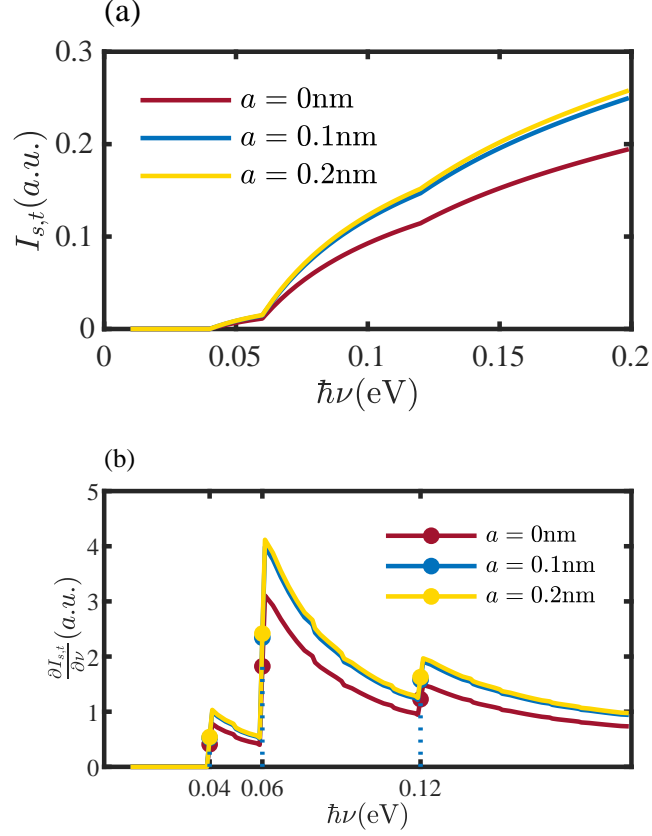


Figure 5: (a) The zero-frequency component of the inelastic tunneling current as a function of the frequency with the lateral displacement between the tip and the molecule fixed at  $\vec{a} = (0,0,d)$ ,  $\vec{a} = (0.1\text{nm},0,d)$  and  $\vec{a} = (0.2\text{nm},0,d)$ , which is represented by the red, blue and yellow curves respectively. (b) The first derivative of the zero-frequency component of the current with respect to the frequency. The correspondence between the color and the lateral displacement is the same as (a). The dotted markers show the discontinuous spots in curves. The other parameters are the same as before.

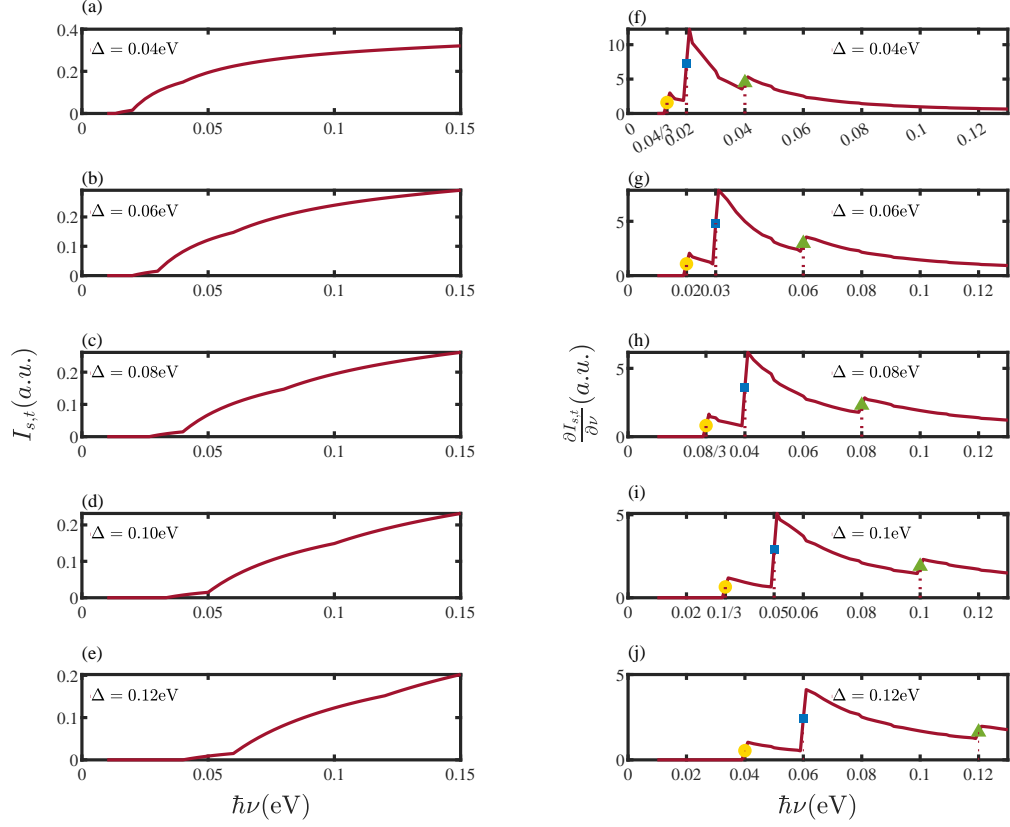


Figure 6: The inelastic tunneling current and its first derivative in  $\vec{a} = (0.2\text{nm}, 0, d)$  with  $\Delta = 0.04, 0.06, 0.08, 0.1, \text{ and } 0.12\text{eV}$ . (a)-(e) show the inelastic tunneling current with an upward trend. (f)-(j) give the first derivative of the current. The round (square, triangle) dot characterizes the discontinuous points.



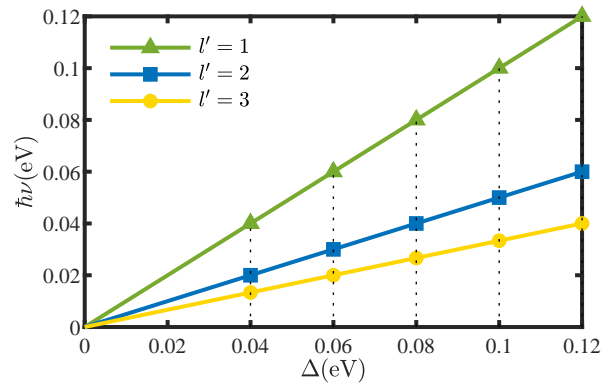


Figure 7: The energy of knee points as a function of  $\Delta = E_{\text{eg}} + eV_0$ . The data points in round (square, triangle) correspond to the knee points with the same marker in Fig. 6. The slope of the triangle (square, round) dot line equals to  $1/l' = 1$  ( $1/2, 1/3$ ).